Journal of Power Sources 270 (2014) 434–440

Contents lists available at ScienceDirect

Journal of Power Sources

journal homepage: www.elsevier.com/locate/jpowsour

Reduction kinetics of iron-based oxygen carriers using methane for chemical-looping combustion

Ming Luo, Shuzhong Wang*, Longfei Wang, Mingming Lv

Key Laboratory of Thermo-Fluid Science and Engineering of MOE, School of Energy and Power Engineering, Xi'an Jiaotong University, Xi'an 710049, China

HIGHLIGHTS

- The performance of three iron-based oxygen carriers in reduction process using methane are investigated.
- The reaction mechanism between the oxygen carriers and methane is investigated.
- Increasing reaction temperature increases the conversion rate of the oxygen carriers.
- Iron ore and synthetic $Fe_2O_3/MgAl_2O_4$ show better stability than that of pure Fe_2O_3.

ARTICLE INFO

Article history:
Received 22 April 2014
Received in revised form
12 July 2014
Accepted 15 July 2014
Available online 30 July 2014

Keywords:
Kinetic
Methane
Chemical-looping
CO_2 capture
Iron oxides
Oxygen carrier

ABSTRACT

The performance of three iron-based oxygen carriers (pure Fe_2O_3, synthetic $Fe_2O_3/MgAl_2O_4$ and iron ore) in reduction process using methane as fuel is investigated in thermo-gravimetric analyzer (TGA). The reaction rate and mechanism between three oxygen carriers and methane are investigated. On the basis of reactivity in reduction process, it may be concluded that $Fe_2O_3/MgAl_2O_4$ has the best reactivity with methane. The reaction rate constant is found to be in the following order: $Fe_2O_3/MgAl_2O_4$ > pure Fe_2O_3 > iron ore and the activation energy varies between 49 and 184 kJ mol^{-1}. Reduction reactions for the pure Fe_2O_3 and synthetic $Fe_2O_3/MgAl_2O_4$ are well represented by the reaction controlling mechanism, and for the iron ore the phase-boundary controlled (contracting cylinder) model dominates. The particles of iron ore and synthetic $Fe_2O_3/MgAl_2O_4$ have better stability than that of pure Fe_2O_3 when the reaction temperature is limited to lower than 1223 K. These preliminary results suggest that iron-based mixed oxygen carrier particles are potential to be used in methane chemical looping process, but the reactivity of the iron ore needs to be increased.

1. Introduction

With an increasing expansion of the vehicle population, the reduction of carbon dioxide and the pollutants emission during the combustion process have become the focus of attention around the world. In 2011, transport sector was the second-largest sector to emit carbon dioxide, which represented 22% of global CO_2 emissions [1]. Meanwhile, the pollutant emissions from the vehicles have become the main resource in the urban areas, especially for China [2,3]. Therefore, emissions reduction in the transport sector is one of the urgent problems.

Hydrogen appears to be one of the most promising energy carriers due to its potentially higher energy efficiency and low generation of pollutants, which can be used as the fuel in fuel cells, such as the proton exchange membrane fuel cells (PEMFCs). Steam reforming process of methane (SMR) is now the most widely used technology for H_2 production in the industrial scale [4]. Although it is wildly used in hydrogen generation, SMR process involves many complex catalytic steps. Moreover, to sustain the endothermic reactions, heat is supplied by burning part of the natural gas or the purge gas from the PSA in a furnace. Therefore, this process cannot achieve a 100% CO_2 capture rate.

Steam reforming using chemical-looping (CLR(s)) was originally proposed by Mattissson and Lyngfelt et al. [5] in 2001. The Schematic description of CLR(s) is illustrated in Fig. 1. In CLR(s) process, the steam reforming part does not differ from the conventional process in the way that the reactions take place inside tubes using suitable catalysts and working at elevated pressure. However, the

* Corresponding author.
E-mail addresses: luoming_01@stu.xjtu.edu.cn (M. Luo), szwang@aliyun.com (S. Wang), wanglf@stu.xjtu.edu.cn (L. Wang), m.m.lv@stu.xjtu.edu.cn (M. Lv).

http://dx.doi.org/10.1016/j.jpowsour.2014.07.100
0378-7753/

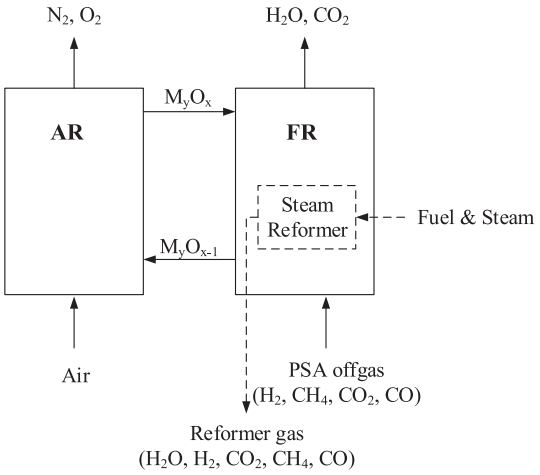

Fig. 1. Schematic description of CLR(s).

tubes are placed inside the fuel reactor (FR) in a chemical looping combustion (CLC) unit. Hence, the tubes are heated by the oxygen carrier particles from the air reactor but not by direct firing outside of the tubes. The offgas from the steam reforming including CH_4, CO_2, CO and H_2 is used as the feed gas to the FR. The output gas from the FR is the mixture of CO_2 and H_2O, thus pure CO_2 can be easily obtained and captured by condensing H_2O. It can be found that the CLR(s) process combines the traditional steam reforming process and CLC process.

The screening of proper oxygen carriers is the basis of successful operation in the CLR(s) process. Iron has been widely investigated as one of the proper oxygen carriers in the CLC process due to its high mechanical strength and high stability at high temperature [6]. It is also environmental-friendly with relatively low cost, and there is also no thermodynamic limitation in converting gaseous fuel and no risk of sulphide or sulphate formation [7]. Several works have shown that Fe-based oxygen-carriers also have enough reactivity both at atmospheric [8–11] and pressurized conditions [12] especially for H_2 and CO. However, the low oxygen transport capacity and the relatively low reactivity with methane are the key drawbacks of the Fe-based oxygen carriers. To obtain high fuel conversion of the offgas from the steam reforming, the reactivity of the iron-based oxygen carriers with methane should be promoted. The reactivity and the stability of the iron based oxygen carriers can be increased with inert addition [13–15], but the synthetically produced particles have a significantly higher production cost. Therefore, the low-cost natural iron-based ores have attracted significant interest because they are much cheaper and easily obtained. The feasibility of some inexpensive materials as oxygen carrier materials in CLC process such as ilmenite, iron ore, and industrial products containing iron oxide has been proved in some literature [16–23].

Most of the fuels used to study the reactivity of the iron-based oxygen carriers are H_2 and/or CO [12,24]. However, the reduction mechanism of the iron-based oxygen carriers using methane as fuel has been seldom investigated [25], and therefore there is a great need to investigate the kinetics of iron-bases oxygen carrier materials with methane. In this paper, pure Fe_2O_3, supported hematite Fe_2O_3 and iron ore were selected as oxygen carriers and methane as fuel. The reaction rate and its mechanism between three oxygen carriers and methane were investigated. To determine the reduction kinetics with methane, the experiments were carried out in TGA and the obtained data were analyzed by various gas–solid reaction models.

2. Experimental section

2.1. Materials

The pure iron oxide and the supported oxygen carrier $Fe_2O_3/MgAl_2O_4$ used in this paper were prepared by mechanical mixing. The mass ratio of $Fe_2O_3/MgAl_2O_4$ equals to 80:20, and this oxygen carrier is denoted by Fe_8Mg_2. The preparation process of the inert material $MgAl_2O_4$ and the synthetic oxygen carrier Fe_8Mg_2 can be found in our previous study [26]. Commercial pure iron oxide powders from the manufacturer (Sinopharm Chemical Reagent Co., Ltd.), with a purity of 99.0% were used in this study.

The iron ore particles from Inner Mongolia were also selected as oxygen carriers. To make sure that the iron ore particles were in their most oxidized state, they were firstly heated in air for 24 h at 1223 K before crushed and sieved to the desired particle size. The composition analysis of the iron ore after heat treated is listed in Table 1. The materials with the size range of 100–200 μm were prepared and tested in this study. The BET surface areas of pure Fe_2O_3, synthetic Fe_8Mg_2 and iron ore are shown in Table 2.

2.2. Experimental procedure

The experimental study was carried out in a TGA system (WCT-2C) produced by Beijing Optics Instrument Factory. The schematic diagram of experimental apparatus has been presented before [27,28].

10 mg oxygen carrier was used in every experiment. The oxygen carrier was loaded in a ceramic pan of the TGA and heated to the predetermined temperature at a heating rate of 20 K min^{-1} in N_2 atmosphere. Then the mixture of methane and CO_2 was introduced and maintained at that condition for 25 min. When the reduction process finished the gas was switched to nitrogen. The reduced oxygen carrier particles were cooled in the nitrogen flow to ambient temperature and collected for further analyses.

The purity of the methane used was higher than 99.99%, while the purity of the N_2 and CO_2 were both higher than 99.9%. In all experiments the flow rate of the reaction gas (CH_4) was set as 40 mL min^{-1} and for inert gas (N_2 or CO_2) it was 60 mL min^{-1} to make the effect of gas film diffusion negligibly small.

2.3. Characterization of the oxygen carrier

Scanning electron microscope (SEM) was performed to investigate the behavior of the oxygen carrier particles with a JSM-6390A microscope. The BET surface areas of the particles were measured using a nitrogen BET analyzer (V-sorb 2008P) produced by Gold APP Instrument Corporation.

2.4. Data evaluation

The fractional reduction conversion during the reduction process was calculated using the TGA data, which was defined as.

$$X = \frac{m_{ox} - m_t}{m_{ox} R_0 x_{MeO}} \quad (1)$$

where m_t is the instantaneous weight of the oxygen carrier sample. R_0 is the oxygen ratio, which is defined as $R_0 = (m_{ox} - m_{red})/m_{ox}$. m_{ox} and m_{red} are the weight of the completely oxidized sample and the reduction form of oxygen carrier after reaction respectively, and x_{MeO} is the fraction of active metal oxide in the sample.

It should be noted that, iron compounds have four different oxidation states (Fe_2O_3–Fe_3O_4–FeO–Fe). Depending on the reducing agency and the gas composition, the reduction of Fe_2O_3

Table 1
Chemical analysis of the iron ore sample.

Components	Fe_2O_3	SiO_2	Al_2O_3	P_2O_5	MnO	MgO	K_2O	TiO_2	SO_3	Cr_2O_3	V_2O_5	Others
Content (wt%)	82.93	6.97	0.924	0.024	0.037	5.146	0.056	0.306	0.186	0.027	0.007	3.387

can finish in one of the above products. In a real CLC system, when methane was used as fuel, H_2O will be produced during the Fe_2O_3 reduction with CH_4, and extra steam may also need to be added to the system for preventing the carbon deposition. Therefore, the final product would normally be Fe_3O_4 due to the thermodynamic equilibrium. Because feeding steam to our TGA apparatus was problematic experimentally, CO_2 was introduced during the reduction process to inhibit the carbon deposition in this paper. FeO may also appear when CH_4–CO_2 was used for the reduction. However, only the transformation from hematite to magnetite (Fe_2O_3–Fe_3O_4) may be applicable for industrial CLC systems. Further reduction to FeO would produce a high decrease in the CO_2 purity obtained in the fuel reactor due to the increase in the equilibrium concentrations of CO and H_2. Because it was not possible to stop the reaction in the Fe_3O_4 product in the TGA system, the reduction form of oxygen carrier was set to Fe_3O_4 when X was calculated, and the first period of the experimental curves from Fe_2O_3 to Fe_3O_4 was used to determine the kinetic of the reaction.

2.5. Kinetic models

The sample weight of the oxygen carrier was continuously recorded in a computer during the isothermal process. The data tested was analyzed by the available gas–solid reaction models to find the reaction mechanisms. Using the reduction conversation, the rate of solid–state reaction can be generally described by:

$$\frac{dX}{dt} = kf(X) \tag{2}$$

where X is the reduction conversion of the oxygen carriers, t is reaction time, k is the temperature dependent reaction rate constant, $f(X)$ is a function that represents the reaction mechanism. k is normally assumed to obey the Arrhenius equation:

$$k = k_0 \exp\left(-\frac{E_a}{RT}\right) \tag{3}$$

where k_0 is pre-exponential factor, E_a is the activation energy of the kinetic process, T is absolute temperature and R the universal gas constant.

Hancock and Sharp [29] have described a convenient method for comparing the kinetics of isothermal solid–state reactions. The experimental data can be expressed as the following equations:

$$1 - X = e^{-nt^m} \tag{4}$$

or

$$\ln[-\ln(1-X)] = m \ln t + \ln n \tag{5}$$

Table 2
The BET surface area of fresh and used oxygen carrier particles.

Oxygen carriers	Fresh samples ($m^2\ g^{-1}$)	Used samples ($m^2\ g^{-1}$)			
		1123 K	1173 K	1223 K	1273 K
Fe_2O_3	1.450	1.425	1.303	1.134	0.991
Fe8Mg2	3.672	3.612	3.441	3.030	2.821
Iron ore	0.071	0.075	0.072	0.073	0.062

where m is slope and n is a constant. In this method, the plots of ln $[-\ln(1-X)]$ vs. ln$t$, are used to distinguish reaction mechanisms. Nine kinetic equations can arbitrarily be separated into three groups: the diffusion controlled, boundary-controlled (nth-order process) and random nucleation and subsequent growth of nuclei models (Table 3). If $m < 1$, this reaction is in favor of the diffusion processes, whereas if $1 < m < 2$, the phase boundary controlled process is possibly dominant, and if $m > 2$, the possibly dominant process is subsequent growth of nuclei process. The best fitting model can be found using the least square method by analyzing a number of curve points in the set range of conversion.

The relation of the rate constant with the reaction temperature from the model is represented by the Arrhenius plots, and the activation energy and pre-exponential factor of reduction process can be calculated from the slope of ln(k) versus $1/T$ for a given value of conversion ranges.

3. Results and discussion

3.1. Effect of reaction temperature on the reduction conversion of the oxygen carriers

The reduction conversion profiles of the pure Fe_2O_3, synthetic Fe_8Mg_2 and iron ore using methane during the reduction process at different temperatures (T = 1123, 1173, 1223, and 1273 K) are shown in Fig. 2. In general, an increase in the reaction temperature yields an increase in the conversion rate of three oxygen carriers. However, when the temperature increases from 1223 K to 1273 K, X of pure Fe_2O_3 decrease from 2.347 to 2.250. This may be due to the sintering and agglomeration of the pure iron oxide at high temperatures. As shown in Fig. 2(c), the values of X of iron ore are also very high at 1273 K. The final conversion is almost the same as that when Fe_8Mg_2 is used. The iron ore materials maintain their reactivity during cyclic operation process has been confirmed [17,30]. The inert materials in iron ore may help to maintain the porosity [30].

From Fig. 2(a), it can be found that the reduction process of pure Fe_2O_3 at different temperature has two stages. In the first stage ($X < 1$), the conversion increases monotonously during the early minutes. In the second stage ($X > 1$), the conversion shows a monotonous increase with a lower rate after which the rise

Table 3
Reaction mechanisms and the solid-state reaction rate equations [25,29].

Reaction mechanism	Equations	n
One-dimensional diffusion	$X^2 = kt$	0.62
Two-dimensional diffusion	$(1-X)\ln(1-X) = kt$	0.57
Three-dimensional diffusion (Jander eq.)	$[1-(1-X)^{1/3}]^2 = kt$	0.54
Three-dimensional diffusion (Ginstein-Brounshtein eq.)	$1 - 2X/3 - (1-X)^{2/3} = kt$	0.57
First-order reaction (unimolecular decay law)	$-\ln(1-X) = kt$	1.00
Phase-boundary controlled (contracting cylinder)	$1-(1-X)^{1/2} = kt$	1.11
Phase-boundary controlled (contracting sphere)	$1-(1-X)^{1/3} = kt$	1.07
Two-dimensional growth of nuclei	$[-\ln(1-X)]^{1/2} = kt$	2.00
Three-dimensional growth of nuclei	$[-\ln(1-X)]^{1/3} = kt$	3.00

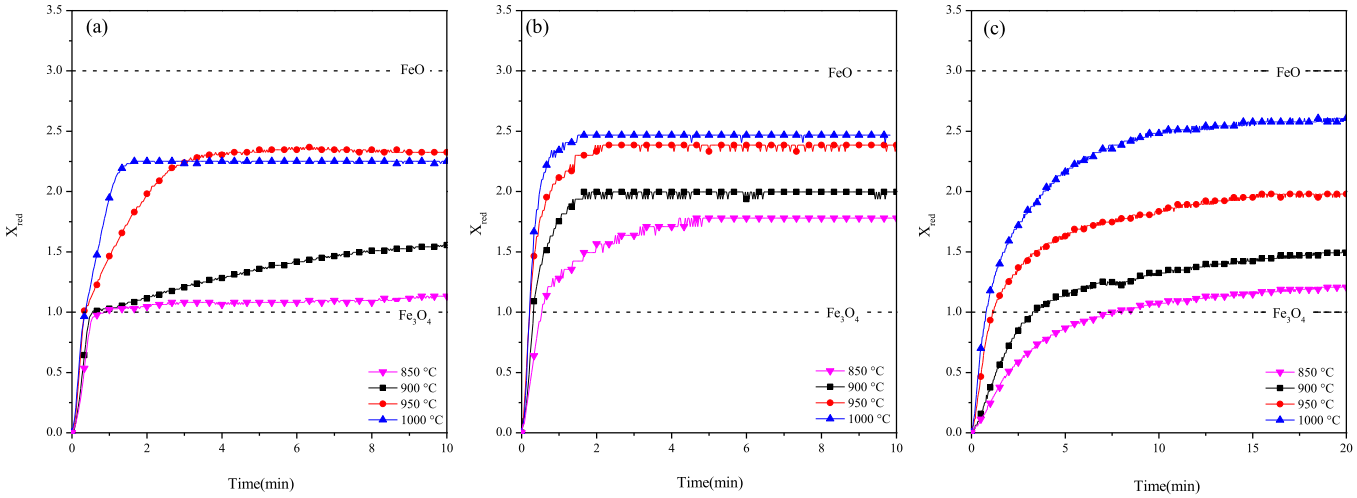

Fig. 2. The conversion curves of different oxygen carriers as a function of time at different temperatures: (a) pure Fe_2O_3, (b) Fe_8Mg_2, (c) iron ore.

gradually slows down. The two stages in conversion imply that the reduction process of the pure Fe_2O_3 is reduced in two steps as $Fe_2O_3 \rightarrow Fe_3O_4 \rightarrow FeO$, and the reduction rate from Fe_2O_3 to Fe_3O_4 is higher than that from Fe_3O_4 to FeO. As can be seen from Fig. 2(a) and (b), the conversion curves are almost the same at the first stage of the reduction process at both 1223 K and 1273 K, which means that the reduction process from Fe_2O_3 to Fe_3O_4 is temperature independent at high temperatures. This is in accordance with the conclusion obtained by Go et al. [25]. They found that the effect of the temperature was insignificant in the region from hematite (Fe_2O_3) to magnetite (Fe_3O_4).

After the comparison of three oxygen carriers at different temperatures, it can be found that the reactivity of the synthetic oxygen carrier Fe_8Mg_2 is best for methane conversion which is no surprise since it is one of the best iron-based oxygen carriers designed for methane conversion [15]. The values of X increase with the addition of inert support. A possible explanation for it is that the surface areas increase with the addition of inert support and the number of active site with methane also increases. Note that, the reactivity of the iron ore needs to be improved. The low reactivity of iron ore may be due to the low BET surface area as mentioned in Section 2.1. However, the iron ore also obtains high conversion at high temperature, and therefore the iron ore has great potential in an industrial CLC process from an economic standpoint.

It should be noted that, there is no weight gain during the reduction process even when the temperature is higher than 1173 K. This indicates that there is no carbon deposition during the process. It is found that the carbon deposition on the surface of iron-based oxygen carrier starts as metal iron (Fe) is produced [31]. However, the conversion of the oxygen carrier is limited to FeO in this paper, and XRD analysis confirms that no Fe appears. Moreover, in the reduction processes, CO_2 was introduced with methane, and the CO_2 may react with the carbon to form CO, which has a high reactivity with Fe_2O_3. Therefore, the carbon formation may act as an intermediate in the reduction process. This is in accordance with the results obtained by Cho et al. [6]. They have proposed that carbon formation is an intermediate in the reduction of nickel oxides.

3.2. Oxygen carrier characterization

The SEM images of three oxygen carriers after reduction at four temperatures (T = 1123, 1173, 1223, and 1273 K) are shown in Fig. 3. The particles of pure Fe_2O_3 used at 1123 K and 1173 K have high porosity and don't agglomerated. However, the sizes of the grains on the surfaces of pure Fe_2O_3 particles increase significantly after reduction process at 1223 K, and severe sintering and high agglomeration among the grains are observed. The porosity of particles at 1273 K decreases remarkably. The loss of reactivity at high temperatures may be due to the particle sintering and loss of porosity as observed in Fig. 3(a). The BET surface area of reduced samples are illustrated in Table 2. It can be found that the surface area of the reduced sample of pure Fe_2O_3 decreases significantly with the increase of the reaction temperature. The particles of Fe_8Mg_2 and iron ore after reduction at 1223 K almost maintain the same morphology as that of the particles at 1123 K, and only minor sintering between the grains is observed. This indicates that the surface changes during reduction reaction are not severe when the oxygen carriers operates at 1223 K. The surface area of Fe_8Mg_2 sample after reaction at 1223 K doesn't decrease significantly compared with that of the fresh sample. Note that, the surface areas of iron ore samples after reaction at the temperatures of 1123 K, 1173 K and 1223 K almost maintain the same as that of the fresh sample as shown in Table 2.

All three oxygen carriers sintered significantly when the reduction temperature is 1273 K. As mentioned before, the expected final product would normally be Fe_3O_4. Increasing the temperature to 1273 K can promote the conversion rate of pure Fe_2O_3, but the sintering and agglomeration would have a negative effect on the cyclic physical performance of the oxygen carrier. Therefore, the recommended reaction temperature is limited to lower than 1223 K. It is necessary to conduct long-term multicycle tests to verify the stability of the particles.

3.3. Reduction mechanism and kinetics of the oxygen carriers with methane

Considering the low reactivity of the iron-based oxygen carrier, the experiments for all three particles were all conducted at temperatures above 1123 K. As mentioned before, the expected final product would normally be Fe_3O_4. To further avoid the effect of carbon deposition, the oxygen carrier conversion is limited to 1. To find the mechanism and the kinetic parameters, m value was calculated from Eq. (5). The obtained m values of pure Fe_2O_3, Fe_8Mg_2 and iron ore are 1.961, 1.931, and 1.359, respectively. Based on these average m values, two-dimensional growth of nuclei

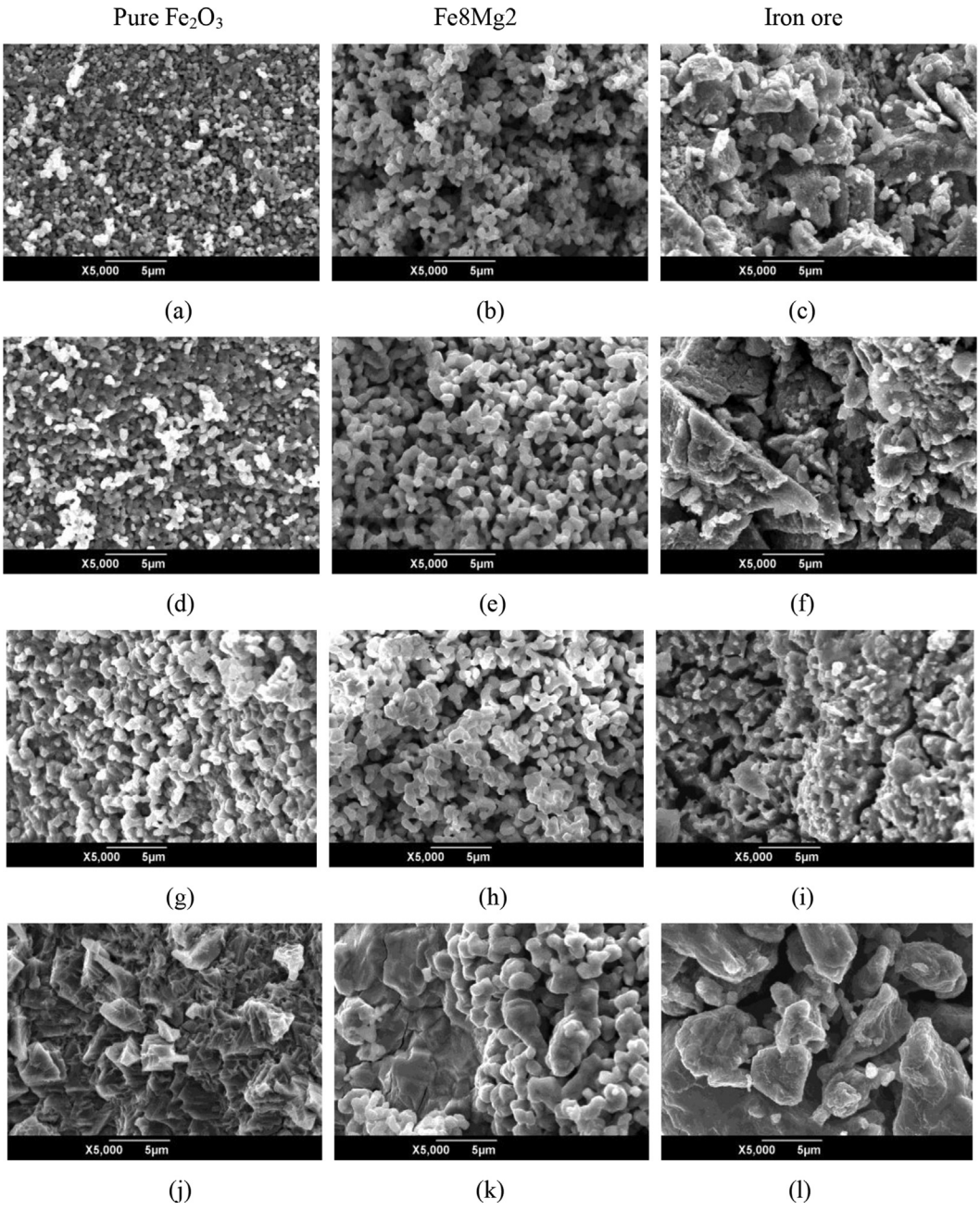

Fig. 3. SEM images of used particles (a, d, g, h: Pure Fe_2O_3; b, e, h, k: Fe_8Mg_2; c, f, i, l: Iron ore) after the reduction process at different temperatures (a, b, c: 850 °C; d, e, f: 900 °C; g, h, i: 950 °C; j, k, l: 1000 °C).

Table 4
The parameters for model fitting in the reduction process with methane.

Oxygen carrier	Pure Fe_2O_3			Fe_8Mg_2			Iron ore		
Reaction model	Two-dimensional growth of nuclei			Two-dimensional growth of nuclei			Phase-boundary controlled (contracting cylinder)		
Temperature (K)	k	m	r	k	m	r	k	m	r
1123	2.897	1.856	0.987	3.096	1.724	0.995	0.127	1.096	0.988
1173	3.888	2.088	0.988	4.806	1.934	0.976	0.270	1.346	0.977
1223	5.168	2.103	0.995	7.781	2.034	0.996	0.783	1.404	0.980
1273	5.247	1.796	0.988	8.009	2.033	0.972	1.160	1.537	0.981

k(/min): reaction rate constant, m: slope of $\ln[-\ln(1-X)]$ vs. $\ln(t)$, r : least square coefficient.

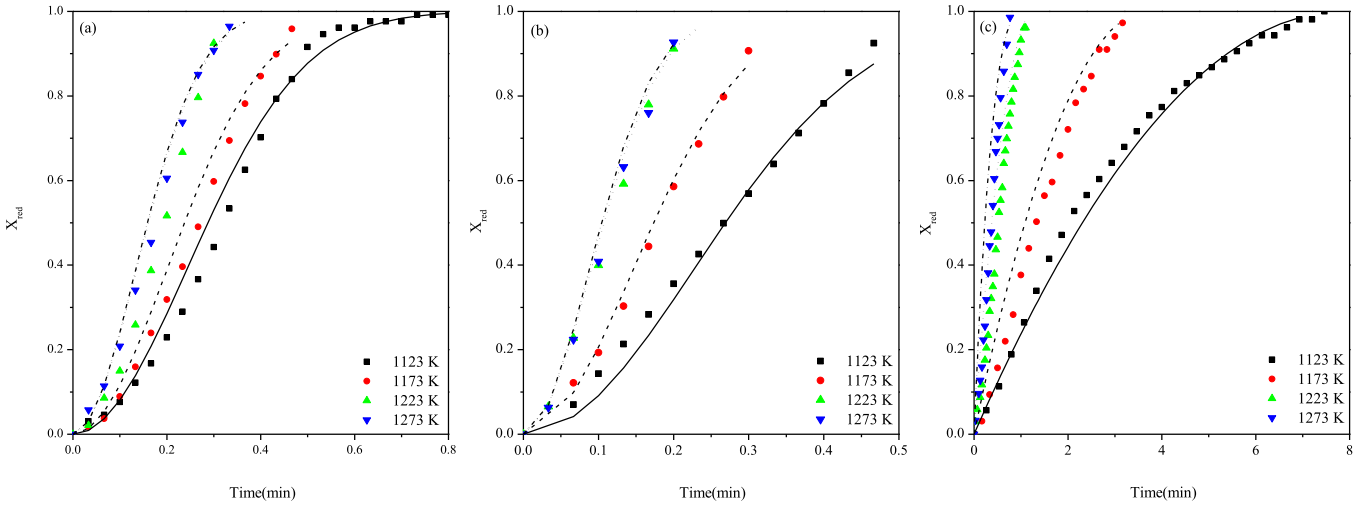

Fig. 4. Comparison of calculated conversion curves with the experimental data: (a) pure Fe_2O_3, (b) Fe_8Mg_2, (c) iron ore.

model is in agreement with the experimental data for pure Fe_2O_3 and Fe_8Mg_2, while the phase-boundary controlled (contracting cylinder) reaction mechanism is the best to predict the experimental data for the reduction of iron ore. The rate constants and the regression coefficients of each metal oxide at different reduction temperatures are summarized in Table 4. It can be found in Table 4 that the reaction rate constant is in the following order: Fe_8Mg_2 > pure Fe_2O_3 > iron ore.

The lines in Fig. 4 represent the curves simulated using the best fitted model for different oxygen carriers during reduction reaction. After comparison of the experimental data with the predicted value for the reduction reaction, it is found that the curve obtained by the chemical reaction control model can predict the experimental results for pure Fe_2O_3 and Fe_8Mg_2. However, for iron ore, there is a small difference between the values of the model predicted and the experimental data. This is due to the average value of m is different compared to the modeling m value, but it can be found that the phase-boundary controlled (contracting cylinder) model can be used to predict the experimental data to a great extent.

Fig. 5 is the Arrhenius diagram of three oxygen carriers for calculation of activation energy. It can be found that, the reaction rate constants of the pure Fe_2O_3 and synthetic Fe_8Mg_2 are larger than that of iron ore. This is likely related to higher surface area resulting in the availability of more active sites. The activation energy (E_a) and pre-exponential factor of reduction process can be obtained. The values of E_a yielded for pure Fe_2O_3, synthetic Fe_8Mg_2 and iron ore were 49.62, 79.96, and 183.63 kJ mol^{-1}, respectively. Therefore, the synergetic Fe_8Mg_2 and iron ore have higher activation energies than that of pure Fe_2O_3, which may be due to the additions in Fe_8Mg_2 and iron ore.

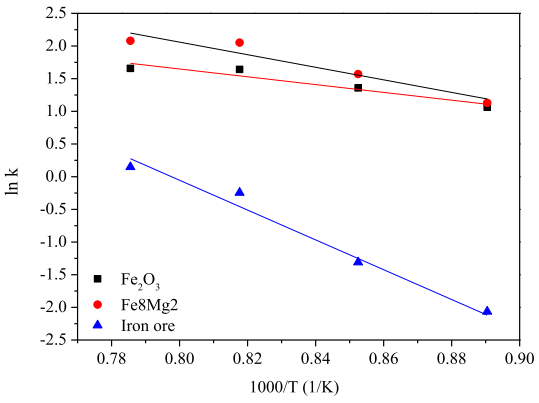

Fig. 5. Arrhenius plot for the calculation of the activation energy.

4. Conclusion

The performance of the iron-based oxygen carriers in reduction process using methane as fuel was preliminarily investigated using TGA. In general, an increase in the reaction temperature produces an increase in the conversion rate of the oxygen carriers.

On the basis of reactivity in reduction process, it may be concluded that carriers prepared with $MgAl_2O_4$ as inert supports has the best reactivity with methane. The reaction rate constant is found to be in the following order: Fe_8Mg_2 > pure Fe_2O_3 > iron ore and the activation energy varies between 49 and 184 kJ mol^{-1}. Reduction reactions for the pure Fe_2O_3 and synthetic Fe_8Mg_2 are well represented by the reaction controlling mechanism while for the iron ore phase-boundary controlled (contracting cylinder) model dominates.

Severe sintering and high agglomeration among the grains on the surfaces of pure Fe_2O_3 particles are observed after reduction process at 1223 K, while the particles of Fe_8Mg_2 and iron ore after reduction at 1223 K almost maintain the morphology. All three oxygen carriers sinter significantly when the reduction temperature is at 1173 K, and therefore the recommended reaction temperature is limited to lower than 1223 K.

Overall, this paper studied the reduction reaction mechanism of three iron-based oxygen carriers with methane which has been seldom investigated for chemical looping combustion. These preliminary results suggest that iron-based mixed oxygen carrier particles are potential to be used in methane chemical looping process, but the reactivity of the iron ore needs to be increased.

Acknowledgments

This work was supported by the National Science and Technology Supporting Program of China (2011BAK06B04) and the Program for New Century Excellent Talents in University of Chinese Education Ministry (NCET-07-0678).

References

[1] M. van der Hoeven, CO_2 Emissions from Fuel Combustion Highlights, International Energy Agency, France, 2013.
[2] K. He, H. Huo, Q. Zhang, Annu. Rev. Energy Environ. 27 (2002) 397–431.
[3] L. Fu, J. Hao, D. He, K. He, P. Li, J. Air Waste Manage. Assoc. 51 (2001) 658–668.
[4] R. Kothari, D. Buddhi, R.L. Sawhney, Renew. Sust. Energy Rev. 12 (2008) 553–563.
[5] T. Mattisson, A. Lyngfelt, Applications of chemical-looping combustion with capture of CO_2, in: Proc. 2nd Nordic Minisymposium on Carbon Dioxide Capture and Storage, 2001. Göteborg, Sweden.
[6] P. Cho, T. Mattisson, A. Lyngfelt, Ind. Eng. Chem. Res. 44 (2005) 668–676.
[7] E. Jerndal, T. Mattisson, A. Lyngfelt, Chem. Eng. Res. Des. 84 (2006) 795–806.
[8] J. Adanez, L.F. de Diego, F. Garcia-Labiano, P. Gayan, A. Abad, J.M. Palacios, Energy Fuel 18 (2004) 371–377.
[9] A. Abad, J. Adanez, F. Garcia-Labiano, L.F. de Diego, P. Gayan, J. Celaya, Chem. Eng. Sci. 62 (2007) 533–549.
[10] T. Mattisson, M. Johansson, A. Lyngfelt, Energy Fuel 18 (2004) 628–637.
[11] M. Johansson, T. Mattisson, A. Lyngfelt, Ind. Eng. Chem. Res. 43 (2004) 6978–6987.
[12] F. Garcia-Labiano, J. Adanez, L.F. de Diego, P. Gayan, A. Abad, Energy Fuel 20 (2006) 26–33.
[13] C. Shiyi, S. Qiliang, X. Zhipeng, S. Xiaoyan, X. Wenguo, Int. J. Hydrogen Energy 36 (2011) 8915–8926.
[14] G.T. Jin, H.J. Ryu, S.H. Jo, S.Y. Lee, S.R. Son, S.D. Kim, Korean J. Chem. Eng. 24 (2007) 542–546.
[15] M.T. Johansson, A. Lyngfelt, Therm. Sci. 10 (2006) 93–107.
[16] H. Leion, T. Mattisson, A. Lyngfelt, Energy Fuel 23 (2009) 2307–2315.
[17] H. Leion, E. Jerndal, B.M. Steenari, S. Hermansson, M. Israelsson, E. Jansson, M. Johnsson, R. Thunberg, A. Vadenbo, T. Mattisson, A. Lyngfelt, Fuel 88 (2009) 1945–1954.
[18] N. Berguerand, A. Lyngfelt, Greenh. Gas. Control Technol. 1 (2009) 407–414.
[19] T. Proll, K. Mayer, J. Bolhar-Nordenkampf, P. Kolbitsch, T. Mattisson, A. Lyngfelt, H. Hofbauer, Greenh. Gas. Control Technol. 1 (2009) 27–34.
[20] A. Fossdal, E. Bakken, B.A. Oye, C. Schoning, I. Kaus, T. Mokkelbost, Y. Larring, Int. J. Greenh. Gas. Control 5 (2011) 483–488.
[21] M. Ortiz, P. Gayan, L.F. de Diego, F. Garcia-Labiano, A. Abad, M.A. Pans, J. Adanez, J. Power Sources 196 (2011) 4370–4381.
[22] H.M. Gu, L.H. Shen, J. Xiao, S.W. Zhang, T. Song, Energy Fuel 25 (2011) 446–455.
[23] R. Xiao, Q.L. Song, S.A. Zhang, W.G. Zheng, Y.C. Yang, Energy Fuel 24 (2010) 1449–1463.
[24] J.A. Peña, E. Lorente, E. Romero, J. Herguido, Catal. Today 116 (2006) 439–444.
[25] K.S. Go, S.R. Son, S.D. Kim, Int. J. Hydrogen Energy 33 (2008) 5986–5995.
[26] S.Z. Wang, G.X. Wang, F. Jiang, M. Luo, H.Y. Li, Energy Environ. Sci. 3 (2010) 1353–1360.
[27] S.Z. Wang, M. Luo, G. Wang, L. Wang, M. Lv, Energy Fuel (2012).
[28] M. Luo, S. Wang, L. Wang, M. Lv, L. Qian, H. Fu, Fuel Process. Technol. 110 (2013) 258–267.
[29] J.D. Hancock, J.H. Sharp, J. Am. Ceram. Soc. 55 (1972) 74–77.
[30] H. Kindermann, M. Kornberger, J. Hierzer, J.O. Besenhard, V. Hacker, J. Power Sources 145 (2005) 697–701.
[31] S. Takenaka, N. Hanaizumi, V. Son, K. Otsuka, J. Catal. 228 (2004) 405–416.